Highlights

- A novel source-free domain adaptation method for cross-domain bearing fault diagnosis, balancing feature discriminability and diversity.

- A label voting strategy with data augmentation to classify and effectively utilize reliable and unreliable target samples.

- Superior performance compared to existing source-free methods and competitive results against non-source-free approaches.

Source-free domain adaptation based on label reliability for cross-domain bearing fault diagnosis

Wenyi Wu[a], Hao Zhang[b], Zhisen Wei[c], Xiao-Yuan Jing[a], Qinghua Zhang[a], Songsong Wu[a,*]

[a]*Guangdong Provincial Key Laboratory of Petrochemical Equipment Fault Diagnosis and School of Computer, Guangdong University of Petrochemical Technology, Maoming, 525000, China*
[b]*Shenzhen Institute of Advanced Technology, Chinese Academy of Sciences, Shenzhen, 518055, China*
[c]*Key Laboratory of Data Science and Intelligence Application (Minnan Normal University), Fujian Province, Zhangzhou, 363000, China*

Abstract

Source-free domain adaptation (SFDA) has been exploited for cross-domain bearing fault diagnosis without access to source data. Current methods select partial target samples with reliable pseudo-labels for model adaptation, which is sub-optimal due to the ignored target samples. We argue that every target sample can contribute to model adaptation, and accordingly propose in this paper a novel SFDA-based approach for bearing fault diagnosis that exploits both reliable and unreliable pseudo-labels. We develop a data-augmentation-based label voting strategy to divide the target samples into reliable and unreliable ones. We propose to explore the underlying relation between feature space and label space by using the reliable pseudo-labels as ground-truth labels, meanwhile, alleviating negative transfer by maximizing the entropy of the unreliable pseudo-labels. The proposed method achieves well-balance between discriminability and diversity by taking advantage of reliable and unreliable pseudo-labels. Extensive experiments are conducted on two bearing fault benchmarks, demonstrating that our approach achieves significant performance improvements against existing SFDA-based bearing fault diagnosis methods. Our code is available at https://github.com/BdLab405/SDALR

Keywords: Bearing fault diagnosis, Source-free domain adaptation, Pseudo-label voting, Deep transfer learning

1. Introduction

As critical components in rotating equipment, the performance and reliability of rolling bearings are vital for industrial machinery's stable operation and safety [1]. Bearing faults can degrade equipment efficiency or lead to system failures, making fault diagnosis essential across industries such as manufacturing, petroleum refining, and aerospace [2, 3, 4, 5, 6].

Bearing fault diagnos is involves analyzing sensor signals (e.g., vibration, thermal images, acoustic emissions) to assess bearing health [7, 8]. While deep-learning-based methods offer improved accuracy, their reliance on the independence and identical distribution (i.i.d.) assumption between training and test samples limits real-world applicability. To address domain shifts, domain adaptation (UDA) methods transfer cross-domain knowledge for robust diagnostics [9]. Metric-based approaches minimize domain discrepancies using measures like Maximum Mean Discrepancy (MMD) [10], KL divergence [11], and Wasserstein distance [12]. Adversarial-based methods use Generative Adversarial Networks (GANs) to extract domain-invariant features [13].

Despite their effectiveness, UDA-based methods require access to source data, which is often impractical due to privacy concerns, storage, and computational burdens [14, 15]. Source-Free Domain Adaptation (SFDA) addresses these limitations by adapting pre-trained source models to target domains without source data. Unlike conventional UDA methods, which rely on both source and target data to reduce domain discrepancies, SFDA enables compliance with data privacy regulations while reducing storage and computational demands, making it a practical solution for real-world applications (illustrated in Figure 1).

Although different strategies such as self-training [16], contrastive learning[17], clustering[18] and data generation[19] have been studied for SFDA.

Specifically, current SFDA-based bearing fault diagnosis approaches are prone to three nonnegligible ob-
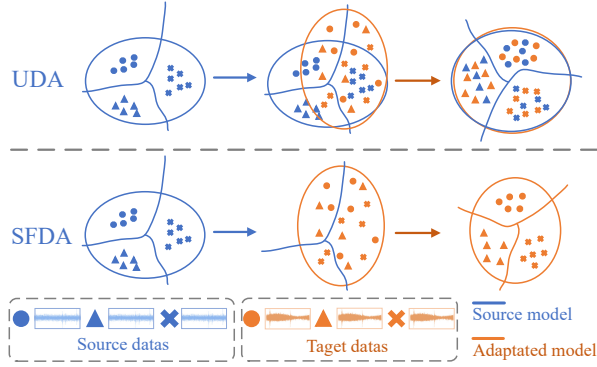
Figure 1: Domain Adaptation and Source Free Unsupervised Domain Adaptation.

stacles (1) In bearing fault diagnosis, maintaining a balance between discriminability and diversity is essential for effective domain adaptation. SHOT[20], a foundational SFDA approach, emphasizes this principle and has been widely adopted by subsequent methods[21, 22]. However, many methods achieve a "fake balance" by relying solely on predicted target sample labels, ignoring the structural characteristics of target data and their role in label prediction. This limitation is particularly critical in fault diagnosis, where signal features are highly variable. (2) Vibration signals in bearing fault diagnosis are typically nonstationary, noisy, and influenced by operational conditions, exacerbating pseudo-label noise. Consequently, the reliability assessment of target pseudo-labels with the statistics of pseudo-labels, such as entropy[23], can be inaccurate. Misclassified samples with high confidence often mislead the adaptation process, reducing the model's ability to accurately identify faults. (3) Distinguishing the importance of target samples is crucial in SFDA-based fault diagnosis. Due to the inherent correlations among vibration signals, unreliable samples often share features with reliable ones. While existing methods[23, 24] prioritize reliable samples to improve adaptation, they tend to overlook the proper handling of unreliable samples. Inadequately processing these samples increases the risk of negative transfer, hindering the model's overall performance.

In this paper, we present a label-reliability-based source-free domain adaptation approach (SDALR) to address the above three issues: (1) We propose exploring the relation between feature space and label space to balance discriminability and diversity during model adaptation. The core principle is to ensure that the model produces similar features for samples sharing the same label and generate distinct features for samples with different labels. (2) To accurately assess the reliability of predicted labels in the target domain, we propose a pseudo-label voting strategy based on data augmentation. The strategy consists of separately predicting the class labels for each augmented sample and integrating the multiple pseudo-label by label voting. As a result, each target sample is given a specific label or is identified as an unreliable sample. (3) To alleviate negative transfer caused by the unreliable target samples, we propose to maximize the entropy of their predicted labels for less classification bias. In so doing, model adaptation is dominated by the increasing reliable samples and free from the inference of unreliable samples.

In summary, the contributions of this paper are as follows:

1. We propose a novel source-free domain adaptation approach for cross-domain bearing fault diagnosis that explores the relation between vibration features and fault labels with well-balance between discriminability and diversity.

2. We propose separate constraints on reliable and unreliable target samples which are obtained by our label voting strategy with data augmentation so that all target samples can be used for cross-domain adaptation.

3. We empirically show the advantage of our approach over existent source-free methods for cross-domain bearing fault diagnosis and provide evidence for competitive performance against existing non-source-free works.

The remainder of the paper is structured as follows. Section 2 introduces the related work. Section 3 describes details about the proposed method. Next, Section 4 reports the comprehensive experimental findings. At last, Section 5 concludes this study.

2. Related Work

2.1. Diagnostic Methods Based on Unsupervised Domain Adaptation

UDA methods generally require access to source data during the adaptation process. These approaches involve supervised learning on labeled source data while simultaneously measuring and reducing the distributional discrepancies between the source and target domains. Rooted in statistical learning theory, UDA techniques have been widely applied to various computer vision tasks [25]. By bridging these gaps, knowledge can be effectively transferred from the source domain to the target domain, enabling accurate predictions for unlabeled target data. Research in this area typically falls

2

into two primary categories: metric-based methods and adversarial-based methods.

Metric-based methods, like MMD [26] and CORAL [27], minimize distributional discrepancies through statistical measures. Wen et al. used MMD to extract domain-invariant features, while Qian et al. employed higher-order KL divergence for comprehensive moment alignment [28]. Ferracuti et al. applied Wasserstein distance for machine condition analysis [29] and Chen et al. introduced UDAD to enhance knowledge transfer with mutual information maximization [30]. Li et al. developed central moment metrics for precise fault diagnosis under varying conditions [31].

Adversarial-based methods, inspired by GANs [32], automate feature extraction via adversarial training. Wang et al. integrated Wasserstein distance and domain classifiers in deep adversarial transfer learning [33], while Kuang et al. combined self-supervised learning with dual classifiers [34]. Zhao et al. incorporated attention mechanisms into a multi-scale adversarial framework [35] and Jiao et al. designed a cycle-consistent approach for domain alignment [36]. Additionally, some studies have explored hybrid approaches that combine metric-based and adversarial-based strategies. For instance, Mao et al.'s multi-fault mode network [37] and Zhou et al.'s adaptive transfer framework [38], blend metric- and adversarial-based strategies for dynamic alignment. Despite these advancements, traditional UDA's reliance on source data poses privacy challenges in sensitive contexts.

While traditional UDA methods have significantly advanced fault diagnosis under varying working conditions and distribution shifts, their reliance on source data presents notable limitations, particularly in scenarios where data privacy is a critical concern.

2.2. Diagnostic Methods Based on Source-free Domain Adaptation

In bearing fault diagnosis, SFDA focuses on adapting a pre-trained source model to an unlabeled target domain without requiring access to source domain data. This approach addresses the challenge of domain adaptation under restricted access to source data. SFDA is particularly significant in scenarios that demand stringent data privacy protections, as required by regulations such as the EU General Data Protection Regulation (GDPR) [39] and China's Data Security Law[40].

The concept of SFDA was first introduced by Liang [20] in computer vision, SFDA fixes classifier parameters and generates high-confidence pseudo-labels for target data to self-train the feature generator. Building on this, Jiao [41] tailored SFDA for rotating machinery

by combining label generation and nuclear norm regularization to preserve class diversity and enhance diagnostics. Similarly, Zhu [42] and Yue [43] utilized information maximization to improve performance under varying conditions. Zhang [44] expanded SFDA with a universal framework incorporating contrastive learning and self-supervised strategies for class alignment and unknown class rejection.

Clustering has also been investigated as an SFDA strategy, with its notable applications in computer vision serving as inspiration. Drawing from these works, Li [45] developed a convolutional neural network using fault mode clustering and attention mechanisms, while Zhu [23] and Zhang [46] introduced clustering-enhanced label generation approaches to boost diagnostic performance in target domains.

Despite these advancements, challenges remain in fully utilizing knowledge from the source model, generating high-quality pseudo-labels, and enhancing model robustness. The lack of direct reference information from the source model can lead to unstable training processes, potentially compromising model performance and reliability in real-world industrial applications.

3. Proposed Method

3.1. Problem Definition

This study addresses the cross-domain bearing fault diagnosis task as a C-way classification from a labeled source domain to a unlabeled target domain. We are given a source dataset $D_s = \{(x_i^s, y_i^s)\}_{i=1}^{N_s}$ from the source domain, where $x_i^s \in \mathcal{X}$ represents source data and $y_i^s \in \mathcal{Y}$ denotes its corresponding label. Meanwhile, we are also given a target dataset $D_t = \{x_i^t\}_{i=1}^{N_t}$, in which each target sample $x_i^t \in \mathcal{X}$ is sampled from the same data space as D_s but its label $y_i^t \in \mathcal{Y}$ is unknown. In the context of domain adaptation, it is reasonably assumed that a marginal distribution shift exists between the source and target domains, i.e. $p_s(x) \neq p_t(x)$, while their posterio probability is identical, i.e. $p_s(y|x) \approx p_t(y|x)$. With respect to SFDA, a classification model M_s is supervised trained on D_s, then it is adapted into the target domain merely relying on D_t to predict the class labels y_i^t.

The source model is composed of a feature extractor f_s and a classifier g_s, so that class probabilities are obtained by $p_s(x) = M_s(x) = \sigma(g_s(f_s(x)))$ for softmax function σ and the predicted label $\hat{y}$ is provided by pseudo-label voting strategy. For adaptation to the target domain, a target model M_t with the same network architecture as M_s is initialized using the parameters of M_s and then is updated on D_t through knowledge transfer.
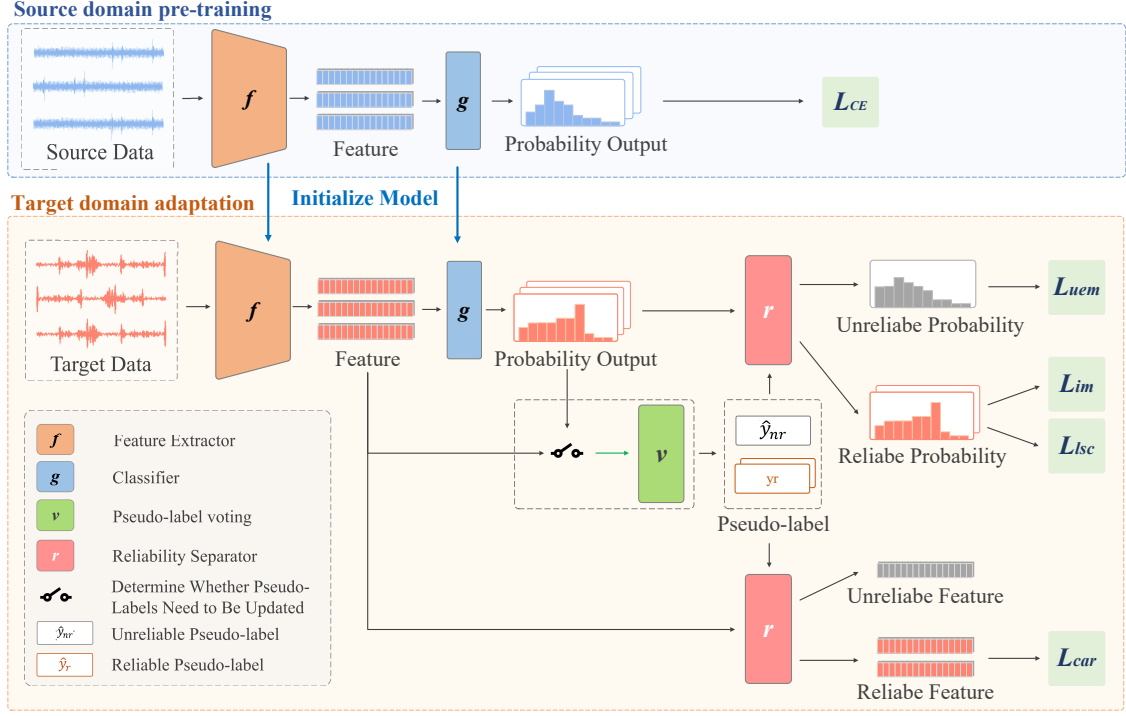
3

Figure 2: The method of SDALR. The source domain training phase is represented by the blue section, while the target domain adaptation phase is represented by the orange section.

3.2. Model Overview

Figure 2 presents the overall workflow of the SDALR method, which is composed of two major stages: the source domain pre-training stage and the target domain adaptation stage.

In the source domain pre-training stage, the source model is trained in a supervised manner using the labeled source domain dataset. Specifically, the model is optimized by minimizing the cross-entropy loss computed over the source domain dataset D_s.

After completing the source domain pre-training, the parameters of the source model M_s are used to initialize the target model M_t and the process transitions to the target domain adaptation phase. During this phase, the target model is fine-tuned using the unlabeled target domain dataset. For pseudo-label generation, a voting strategy based on data augmentation is used, categorizing samples into reliable and unreliable groups. Reliable samples are assigned their corresponding pseudo-labels, while unreliable samples are labeled as -1 to denote their unreliable. For reliable samples, the model is optimized using the cohesion and repulsion loss L_{car}, this loss function promotes the clustering of similar features and the segregation of dissimilar features. Inspired by the SHOT[20] method, a combination

of label-smoothing cross-entropy loss L_{lsc} and information maximization loss L_{im} is used to further refine the model's alignment with reliable samples. For unreliable samples, the entropy maximization loss L_{uem} is applied, which maximizes entropy to limit the certainty of unreliable samples.

3.3. Source Domain Training

In the stage of source domain training, the objective of source domain training is to develop a well-generalized source model M_s, which, after being trained on D_s, serves as the initialization for the target model.

During the training of the source model, the classic cross-entropy loss is used as the optimization objective. The optimization objective can be formulated as follows:

$$L_{CE} = -\mathbb{E}_{x_i^s \in D_s} \sum_{c=1}^{C} q_c \log p^c(x_i^s) \tag{1}$$

where C is the number of classes. q is the onehot encoding of y_i^s so that q_c is '1' for the correct class and '0' for the rest over class c and $p^c(x_i^s)$ denotes the predicted probability of class c for the sample x_i^s, as generated by the source model, also can expressed as $p^c(x_i^s) = \sigma^c(g(f(x_i^s)))$.

4

3.4. Target Domain Adaptation

In target domain adaptation stage, the target model M_t is initialized with the parameters of the pre-trained source model M_s. Subsequently, the adaptation process is performed using the unlabeled target domain dataset. To address this, the study introduces the SDALR approach for effective target domain adaptation.

3.4.1. Pseudo-Label Generation

While some methods assess the reliability of pseudo-labels using statistical metrics, they are often prone to inaccuracies due to noise in the pseudo-labels. To address this, this study proposes an innovative approach. The specific process is shown in Figure 3.

Data augmentation. each sample undergoes n distinct data augmentation transformations, resulting in an expanded set of augmented instances, represented as:

$$X' = \{x, k_1(x), k_2(x), \ldots, k_n(x)\} \tag{2}$$

where $k_1(x), k_2(x), \ldots, k_n(x)$ denote n types of data augmentation methods. In this study, we apply three specific augmentation techniques: flipping, random zeroing, and cyclic shifting. Consequently, the set is given by: $X' = \{x, k_1(x), k_2(x), k_3(x)\}$, where $k_1(x)$, $k_2(x)$, and $k_3(x)$ correspond to flipping, random zeroing, and cyclic shifting, respectively.

Label prediction. We adopt a strategy combining prototype-based (class-wise feature center) calculations with confidence filtering, aiming to generate more reliable pseudo-labels.

Specifically, the initial prototype for each class is calculated by integrating the predicted probabilities (Softmax outputs) and the corresponding feature vectors of target domain samples. The prototype n_c for class c is computed as follows:

$$\eta_c = \frac{\sum_{i=1}^{N_t} p^c(x_i^t) f(x_i^t)}{\sum_{i=1}^{N_t} p^c(x_i^t)} \tag{3}$$

where $f(\cdot)$ represents the feature vector of a sample, $p^c(\cdot)$ denotes the predicted probability for class c and $p^c(x_i^t)$ probability of sample x_i^t belonging to class c.

With the class-wise prototypes computed, initial pseudo-labels are assigned based on a similarity threshold. The similarity metric measures the alignment of a sample's feature vector with its corresponding class prototype. A sample's initial pseudo-label $\hat{y}^0(x)$ determined as:

$$s_c(x) = \frac{f(x) \cdot \eta_c}{\| f(x) \| \| \eta_c \|} \tag{4}$$

$$\hat{y}^0(x) = \begin{cases} \arg\max_c s_c(x), & \text{if} \max_c s_c(x) > \partial \\ -1, & \text{otherwise} \end{cases} \tag{5}$$

where $s_c(x)$ resents the cosine similarity between the feature vector $f(x)$ and the prototype n_c, with $\|\cdot\|$ denoting the Euclidean norm. The threshold ∂ determines whether a pseudo-label is assigned; samples below this threshold are labeled as -1, indicating an unreliable sample.

Label voting. Using the formula above, we compute the label set for each sample in the augmented set X'. The label set is expressed as:

$$\hat{Y}' = \{\hat{y}_0^0(x), \hat{y}_1^0(x), \hat{y}_2^0(x), \ldots, \hat{y}_n^0(x)\} \tag{6}$$

where $\hat{y}_n^0(x)$ is the pseudo-label for the augmented instance $k_n(x)$ and $\hat{y}_0^0(x)$ corresponds to the original sample x. These labels are aggregated using a majority voting strategy. The final pseudo-label $\hat{y}$ is determined as:

$$\hat{y} = \begin{cases} \arg\max_k \left(\sum_{j=1}^m \mathbb{I}(\hat{y}_j^0 = k) \right), & \text{if} \max \left(\sum_{j=1}^m \mathbb{I}(\hat{y}_j^0 = k) \right) > \frac{m}{2} \\ -1, & \text{otherwise} \end{cases} \tag{7}$$

where m denotes the number of pseudo-labels in the voting process and $\mathbb{I}(\cdot)$ is an indicator function that outputs 1 if the condition is true and 0 otherwise. According to this formula, a pseudo-label is finalized if it receives more than half the votes; otherwise, the sample is assigned -1.

To mitigate the adverse effects of imbalanced pseudo-label distributions, this study leverages data augmentation techniques to generate additional samples, thereby achieving a balanced pseudo-label distribution. Specifically, for classes with fewer samples, excluding the label -1, a subset of samples is randomly duplicated and each duplicated sample undergoes one of several randomly selected augmentation methods, including flipping, random masking, or circular shifting. This approach ensures that the number of samples in each class is balanced.

3.4.2. Label-Smoothing Cross-Entropy Optimization

To address the noise and uncertainty introduced during pseudo-label generation, we use a self-training approach with a label-smoothing cross-entropy loss L_{lsc}. The objective function for this process is defined as follows:

$$L_{lsc} = -\mathbb{E}_{x_i^t \in D_t} \sum_{c=1}^C \mathbb{I}(\hat{y}_i \neq -1) q_{(c,i)}^{ls} \log p^c(x_i^t) \tag{8}$$

where the indicator function $\mathbb{I}(\hat{y}_i \neq -1)$ acts as a filtering mechanism, excluding samples labeled as -1 from the loss computation. $p^c(x_i^t)$ is the model's predicted probability for class c. $q_{(c,i)}^{ls}$ represents the smoothed
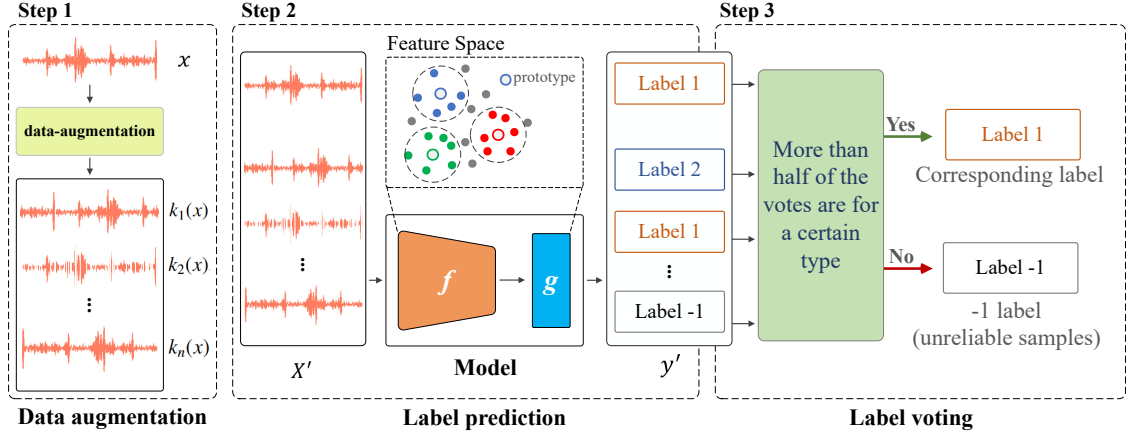
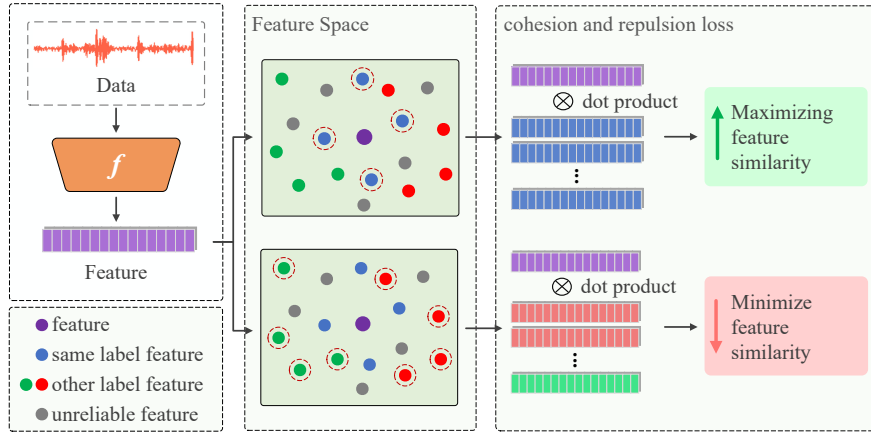5

Figure 3: The specific process of pseudo-label voting

Figure 4: The specific process of cohesion and repulsion

pseudo-label distribution for sample x_i^t in class c, which is defined as:

$$q_{(c,i)}^{ls} = (1 - \alpha)q_{(c,i)} + \frac{\alpha}{C} \qquad (9)$$

where $q_{(c,i)}$ is the one-hot encoding of the pseudo-label $\hat{y}_i$ assigned to sample x_i^t, α is a coefficient controlling the degree of smoothing and α is generally defined as 0.1.

3.4.3. Unreliable Samples Entropy Maximization

Directly minimizing entropy for Unreliable samples can exacerbate errors, while ignoring them may bias the model toward reliable samples. To address this, we apply entropy maximization for unreliable samples, reducing the model's overconfidence in their predictions. This is captured in the entropy maximization loss L_{uem}:

$$L_{uem} = \mathbb{E}_{x_i^t \in D_t} \left[\mathbb{I}(\hat{y} = -1) \sum_{c=1}^{C} p^c(x_i^t) \log p^c(x_i^t) \right] \qquad (10)$$

where $p^c(x_i^t)$ represents the predicted probability of target sample x_i^t for class c. L_{uem} calculates the entropy for samples where $\hat{y} = -1$, minimizing it to enhance the model's confidence in reliable samples.

3.4.4. Information Maximization

To improve model reliability and achieve balanced class distributions, we draw inspiration from the SHOT[20] framework in handling reliable samples. Specifically, we use an information maximization loss comprising two sub-losses designed. The first sub-loss, L_{ent}, minimizes the prediction entropy for samples with reliable pseudo-labels ($\hat{y} \neq -1$). This encourages the model to make precise and confident decisions for these samples. The second sub-loss, L_{div}, promotes balanced class distributions by penalizing deviations from a uniform distribution across all classes. The mathematical

6

formulations for these sub-losses are as follows:

$$L_{ent} = -\mathbb{E}_{x_i^t \in D_t} \left[\mathbb{I}(\hat{y} \neq -1) \sum_{c=1}^{C} p^c(x_i^t) \log p^c(x_i^t) \right] \quad (11)$$

$$L_{div} = \mathbb{I}(\hat{y} \neq -1) \sum_{c=1}^{C} \hat{p}^c \log \hat{p}^c \quad (12)$$

where $\hat{p}^c$ denotes the mean predicted probability for class c across the target dataset, defined as $\hat{p}^c = \mathbb{E}_{x_i^t \in D_t}[\sigma^c(g(f(x_i^t)))]$.

The IM loss integrates entropy-based constraints and diversity regularization, formulated as:

$$L_{im} = L_{ent} + L_{div} \quad (13)$$

3.4.5. Optimization for Feature Cohesion and Repulsion

During target domain adaptation stage, it is crucial to maintain a balance between feature discriminability and diversity. Neglecting the intrinsic data structure of the target domain and its influence on label predictions limits the model's capacity to effectively balance these two aspects. To address this limitation, we propose the cohesion and repulsion loss L_{car}. The specific process is shown in Figure 4.

For each target sample x_i^t with reliable predicted pseudo-label $\hat{y} \neq -1$, we obtain two sample sets as follows,

1. **Similar set** S_i includes reliable target samples that share the same pseudo-label as x_i^t. In the practical phase of training, S_i is constructed within each mini-batch.

2. **Background set** N_i comprises reliable target samples that do not belong to S_i. In the practical phase of training, N_i consists of reliable samples in each mini-batch with different pseudo-labels of x_i^t.

We define the cohesion and repulsion loss function as:

$$L_{car} = \mathbb{E}_{x_i^t \in X_t} \left[\sum_{x_j^t \in S_i} f(x_i^t)^T f(x_j^t) - \beta \sum_{x_m^t \in N_i} f(x_i^t)^T f(x_m^t) \right] \quad (14)$$

where $f(x_i^t)^T$ represents the transpose of $f(x_i^t)$ and $f(x_i^t)^T f(x_j^t)$ denotes their inner product, measuring similarity. The goal is to maximize the similarity between x_i^t and samples in S_i by maximizing $\sum_{x_j^t \in S_i} f(x_i^t)^T f(x_j^t)$ while simultaneously minimizing the similarity between x_i^t and samples in N_i by minimizing $\sum_{x_m^t \in N_i} f(x_i^t)^T f(x_m^t)$. To mitigate the influence of background features, the parameter β is fixed at a constant value of 0.6.

3.4.6. The overall loss function

In the end, 8, 10, 13 and 14 are conbined for Target Domain Adaptation. The integrated training objective is expressed as follows:

$$L_{tar} = L_{lsc} + L_{uem} + L_{im} + L_{car} \quad (15)$$

The whole process of the proposed method SDALR is shown in Algorithm 1.

Algorithm 1: The process of SDALR

Input: Target domain dataset $D_t = \{x_i^t\}_{i=1}^{N_t}$, threshold ∂, parameter β, source domain model M_s
Output: Transferred target model M_t

1 **for** *each training iteration* **do**
2   **if** *pseudo-labels need updating* **then**
3   Augment D_t to create enhanced sample set X' (Eq.2);
4   Extract features $f(x)$ from D_t using f and calculate centroids η_c (Eq.3);
5   Compute similarity s_c between X' and η_c (Eq.4);
6   Filter outputs $\hat{y}^0$ using threshold ∂ (Eq.5);
7   Update pseudo-labels $\hat{y}_i$ through voting strategy (Eq.7);
8   Generate additional samples for each class, with each additional sample randomly chosen a data augmentation method;
9   Extract features $g(x_i^t)$ and probability outputs $p(x_i^t)$ for target samples x_i^t using M;
10   **if** *label of x_i^t is -1* **then**
11   Calculate loss L_{uem} (Eq.10);
12   **else**
13   Calculate loss L_{lsc} (Eq.8);
14   Calculate loss L_{ent} (Eq.11);
15   Calculate global entropy L_{div} (Eq.12);
16   Compute L_{im} by combining L_{ent} and L_{div} (Eq.13);
17   Retrieve all samples with the same label from the current batch as set S_i;
18   Retrieve all samples with different labels in the current batch as set N_i;
19   Calculate L_{car} using N_i and S_i (Eq.14);
20   Combine L_{lsc}, L_{im}, L_{uem} and L_{car} to compute total loss (Eq.15);
21   Update model M based on total loss;

---

4. Experiments

This section provides a comprehensive evaluation of the proposed SDALR method using two public datasets: the PU dataset and the JNU dataset. The experiments

aim to demonstrate the superiority of SDALR in fault diagnosis tasks compared to existing methods and to analyze its effectiveness under various combinations of loss functions.

4.1. Datasets

Paderborn University (PU) Dataset [47]: The PU dataset is a widely used benchmark in bearing fault diagnosis, providing diverse and complex data across various rolling bearing conditions. It consists of six healthy bearing samples, 12 artificially damaged samples and 14 naturally worn samples generated under accelerated loading. Data was collected at a sampling rate of 64 kHz, with 20 independent measurements per condition, each lasting four seconds. Figure 5 illustrates the data collection platform. This study targets eight bearing types for classification: one healthy bearing (K001) and seven naturally faulted bearings (KA04, KA15, KA22, KA30, KI14, KI17 and KI21). The data length is truncated to 2048, with 2000 samples extracted per class. To evaluate performance under different working conditions, six learning tasks were created based on three domain settings: (1) Rotational speed of 1500 r/min, load torque of 0.1 Nm and radial force of 1000 N; (2) Rotational speed of 1500 r/min, load torque of 0.7 Nm and radial force of 400 N; (3) Rotational speed of 1500 r/min, load torque of 0.7 Nm and radial force of 1000 N. As shown in the Table 1, these configurations are referred to as domains A_1, A_2, and A_3, respectively.
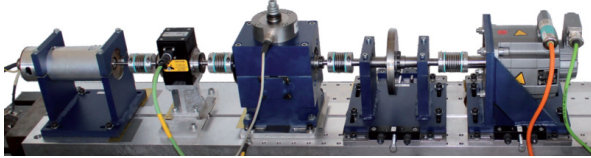

Figure 5: PU[47] experimental platform demonstration

Table 1: The Domain Divisions of Datasets PU

Domain	Parameter combination
A_1	N15_M01_F10
A_2	N15_M07_F04
A_3	N15_M07_F10

Jiangnan University (JNU) Dataset [48]: The JNU dataset, developed by Jiangnan University in China, is an essential resource for bearing fault diagnosis research. It includes four primary bearing types: healthy bearings, bearings with inner ring damage, outer ring damage and rolling element damage, labeled as H, IR,

OR and B, respectively. The data length is truncated to 2048, with 2000 samples extracted per class. Faults were introduced through precision machining, creating micro-indents of 0.3 mm × 0.05 mm (width × depth) on the respective components. Vibration signals were captured using PCB MA352A60 accelerometers at a 50 kHz sampling rate, recording vertical vibrations. The data collection platform is illustrated in Figure 6. As shown in the Table 2, the dataset covers three rotational speed conditions, designated as domains B_1, B_2, and B_3 and supports the construction of six learning tasks.
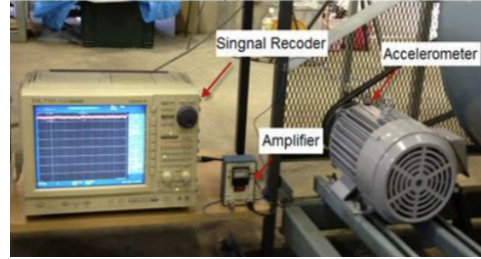

Figure 6: JNU[48] experimental platform demonstration

Table 2: The Domain Divisions of Datasets JNU

Domain	Rotational speed
B_1	600 r/min
B_2	800 r/min
B_3	1000 r/min

4.2. Baselines

The comparative analysis includes a range of transfer learning and domain adaptation strategies, categorized as follows:

Metric-based UDA Methods aim to reduce distributional discrepancies between source and target domains. Joint Adaptation Network (JAN) [49] and Correlation Alignment (CORAL) [27], all of which focus on domain alignment.

Adversarial-based UDA Methods employ adversarial training to achieve domain adaptation and demonstrate strong generalization capabilities. The evaluated algorithms are Domain Adversarial Neural Network (DANN)[50] and Adversarial Discriminative Domain Adaptation (ADDA) [32].

SFDA Methods operate without accessing source domain data. The selected algorithms include Source Hypothesis Transfer (SHOT) [20], a pioneering SFDA

method using pseudo-label cross-entropy and entropy regularization; Source-Free Adaptation Diagnosis (SFAD) [41], which replaces entropy regularization with a kernel matrix loss; and Source-Free Cluster Adaptation (SF-CA) [23], which applies R-drop techniques to improve generalization.

4.3. Implementation Details

The proposed SDALR method was implemented using the PyTorch framework. To ensure fair comparisons, the baseline UDA methods were implemented using the Transfer-Learning-Library, while SHOT, SFAD and SF-CA were independently reproduced.

Network Architecture: This study adopts ResNet-18 as the backbone network, modified specifically for one-dimensional input to accommodate the characteristics of vibration signal data. The network consists of two main modules: a feature extraction module and a classification module. The feature extraction module includes the modified backbone and the intermediate structure, which collectively facilitate hierarchical feature extraction from the input signals. The classification module incorporates a fully connected layer with weight normalization (FC with wn), a technique that re-parameterizes weights into magnitude and direction. This design improves numerical stability during training and accelerates convergence. Detailed network parameters are summarized in Table 3, where Conv represents one-dimensional convolution, BN denotes batch normalization, ReLU indicates the rectified linear unit activation function, ResAdd refers to residual addition and FC stands for fully connected layers.

Experimental Setup: Training employed the stochastic gradient descent (SGD) optimizer with a batch size of 64. For source model training, the initial learning rate was set to 7×10^{-3}, with training spanning 10 epochs. For target model training, a lower learning rate (5×10^{-4} for the PU and JNU dataset) was used to prevent overfitting, extending training to 20 epochs. A dynamic learning rate decay mechanism was implemented as: $\mathrm{lr} = \mathrm{lr}_0 \cdot (1 + 10p)^{0.75}$ where p represents the training progress linearly scaled from 0 to 1 and lr_0 is the initial learning rate.

4.4. Results

The proposed SDALR method was evaluated against baselines on the PU and JNU datasets, with results summarized in Tables 4 and 5. In these tables, "SF" denotes the source-free setting and "$A_1 \rightarrow A_2$" indicates domain adaptation from domain A_1 to A_2. Bolded results indicate the best performance for each task.

Comparison with Traditional UDA Methods: Unlike UDA methods, which require source domain data and raise data privacy concerns, SDALR achieves comparable or superior performance without accessing labeled source data. On the PU dataset, SDALR improves average accuracy by 6.52% over the best UDA method, DANN, and by 1.46% on the JNU dataset.

Comparison with SFDA Methods: Among SFDA methods, SHOT has demonstrated potential in image classification, while SFAD targets multi-feature domain bearing diagnosis. SF-CA enhances target adaptation using conditional autoencoders. However, SDALR consistently outperforms these methods, achieving 5.98% higher accuracy than SF-CA on the PU dataset and 1.09% on the JNU dataset, highlighting its superior adaptability and diagnostic precision.

4.5. Analysis

4.5.1. Classification Performance Analysis via Confusion Matrix

To gain deeper qualitative insights, feature representations were visualized using t-SNE, focusing on the performance of SDALR and the state-of-the-art model SF-CA on two datasets. Tasks $A_1 \rightarrow A_2$, $A_2 \rightarrow A_3$ and $A_3 \rightarrow A_1$ were used for the PU dataset, while tasks $B_1 \rightarrow B_3$, $B_2 \rightarrow B_3$ and $B_3 \rightarrow B_1$ were analyzed for the JNU dataset. Figures 11 and 12 display the feature representations extracted from the final layer of the feature encoder, where different colors correspond to different categories. For the PU dataset, the visualizations cover eight bearing states, while for the JNU dataset, four bearing states are depicted. Unlike traditional unsupervised domain adaptation methods that align features between source and target domains, this study focuses solely on target-domain features due to the source-free adaptation setup. The results show that SDALR learns distinct and well-separated feature representations for each category, enabling precise fault diagnostics. In contrast, SF-CA exhibits less clear class separation.

4.5.2. Hyperparameter Tuning

To assess the impact of hyperparameter selection on the performance of SDALR, experiments were conducted using the PU and JNU datasets, covering all six tasks in each dataset. The analysis focused on two critical hyperparameters: the β value and the ∂ value. The β value determines the weighting of the repulsion component in the L_{car} loss, balancing the aggregation of similar samples with the dispersion of dissimilar samples. The ∂ specifies the similarity criterion used in the pseudo-label voting strategy. During the experiments,

Table 3: Network Architecture Details Of The Proposed Model

Modules	Layers	Parameters	Output Shape
Feature Encoding	Cov → BN	Input channels: 1, Output channels: 64, Kernel size: 7, Stride: 2, Padding: 3	[batch_size, seq_length / 2, 64]
	Conv → BN → ReLU → Conv → BN → ResAdd → ReLU → Conv → BN → ReLU → Conv → BN → ResAdd → ReLU	Output channels: 64, Stride: 1, Padding: 1	[batch_size, seq_length / 2, 64]
	Conv → BN → ReLU → Conv → BN → ResAdd → ReLU → Conv → BN → ReLU → Conv → BN → ResAdd → ReLU	Output channels: 128, Stride: 2, Padding: 1	[batch_size, seq_length / 4, 128]
	Conv → BN → ReLU → Conv → BN → ResAdd → ReLU → Conv → BN → ReLU → Conv → BN → ResAdd → ReLU	Output channels: 256, Stride: 2, Padding: 1	[batch_size, seq_length / 8, 256]
	Conv → BN → ReLU → Conv → BN → ResAdd → ReLU → Conv → BN → ReLU → Conv → BN → ResAdd → ReLU	Output channels: 512, Stride: 2, Padding: 1	[batch_size, 512, seq_length / 16]
	Average Pool → Dropout	Output channels: 1, Dropout rate: 0.1	[batch_size, 1, 512]
	FC → BN		[batch_size, 256, 1]
Classification	FC (with wn) → Softmax		[batch_size, class_number]

Table 4: Diagnosis Results (%) on Dataset PU

Methods	SF	$A_1 \to A_2$	$A_1 \to A_3$	$A_2 \to A_1$	$A_2 \to A_3$	$A_3 \to A_1$	$A_3 \to A_2$	Average
JAN[49]	✗	87.68	92.95	78.67	80.28	90.97	86.8	86.23
CORAL[27]	✗	81.22	91.88	76.81	77.13	90.26	80.02	82.89
DANN[50]	✗	89.69	95.8	83.64	86.07	94.8	90.94	90.16
ADDA[32]	✗	82.73	93.7	75.61	75.4	91.7	80.77	83.32
SHOT[20]	✓	86.41	94.58	82.58	85.12	92.95	87.88	88.25
SFAD[41]	✓	85.33	93.58	80.36	86.23	90.96	86.9	87.23
SF-CA[23]	✓	89.61	96.7	86.47	86.27	95.03	90.71	90.8
LEAD[]	✓	**95.6**	98.4	84.3	84.9	98.9	84.5?	91.1
SDALR	✓	87.03	**99.95**	**96.19**	**99.73**	**99.96**	**97.84**	**96.78**

the ∂ was initially fixed at 0.6 and the β was varied from 0.1 to 1.0 in increments of 0.1. Subsequently, β was fixed at 0.6 and the ∂ was adjusted from 0.5 to 0.95 in increments of 0.05. Figures 9 depict the accuracy trends corresponding to varying β for the PU and JNU datasets, respectively, while Figures 10 illustrate the accuracy variations under different thresholds for both datasets.

The results reveal that, with the threshold fixed at 0.6, the accuracy trends with varying β differ somewhat between the two datasets but share a general pattern: accuracy exhibits an overall upward trend, albeit with fluctuations, as β increases. To address the imbalance in the number of similar and dissimilar samples, adjustments to the hyperparameters were explored to balance their weights. Experimental findings indicate that increasing the weight of the repulsion component for dissimilar samples positively impacts accuracy, underscoring the importance of maintaining clear inter-class distinctions in feature space to enhance model performance.

When the β is fixed at 0.6, threshold ∂ experiments exhibit a consistent trend across both datasets, as shown in the Figure 10. As the threshold increases from 0.5 to 0.95, accuracy initially remains stable but eventually declines. This decline suggests that excessively strict thresholds (e.g., 0.95) overly constrain the selection range of samples, thereby hindering model performance. Conversely, as the threshold becomes less restrictive, accuracy stabilizes, indicating that the current

Table 5: Diagnosis Results (%) on Dataset JNU

Methods	SF	$B_1 \rightarrow B_2$	$B_1 \rightarrow B_3$	$B_2 \rightarrow B_1$	$B_2 \rightarrow B_3$	$B_3 \rightarrow B_1$	$B_3 \rightarrow B_2$	Average
JAN[49]	✗	96.28	96.01	95.1	97.79	91.79	97.57	95.76
CORAL[27]	✗	94.37	92.66	92.75	96.25	89.3	94.73	93.34
DANN[50]	✗	98.46	97.78	95.68	98.37	93.29	98.68	97.04
ADDA[32]	✗	95.7	94.64	85.32	91.37	89.72	95.37	92.02
SHOT[20]	✓	94.31	88.35	90.27	84.37	92.05	97.29	91.11
SFAD[41]	✓	99.14	98.01	94.59	98.43	93.41	99.16	97.12
SF-CA[23]	✓	99.48	98.59	94.71	98.81	93.28	99.6	97.41
LEAD[]	✓	96.1	96.1	92.0	95.4	87.0	91.8	93.0
SDALR	✓	**99.98**	**100**	**96.41**	**100**	**94.71**	**99.92**	**98.50**

Figure 7: Confusion matrix comparison of SF-CA and SDALR on PU datasets to evaluate classification performance across different tasks. Subplot (a)(b)(c) represent the confusion matrices of the SF-CA method, while subplot (d)(e)(f) correspond to the confusion matrices of the SDALR method

sample selection mechanism effectively mitigates the adverse effects of unreliable samples while preserving robust model performance across various threshold settings.

4.5.3. Ablation Studies

Our model is optimized using multiple mechanisms, including cohesion and repulsion loss (L_{car}), pseudo-label voting (voting) and entropy maximization loss
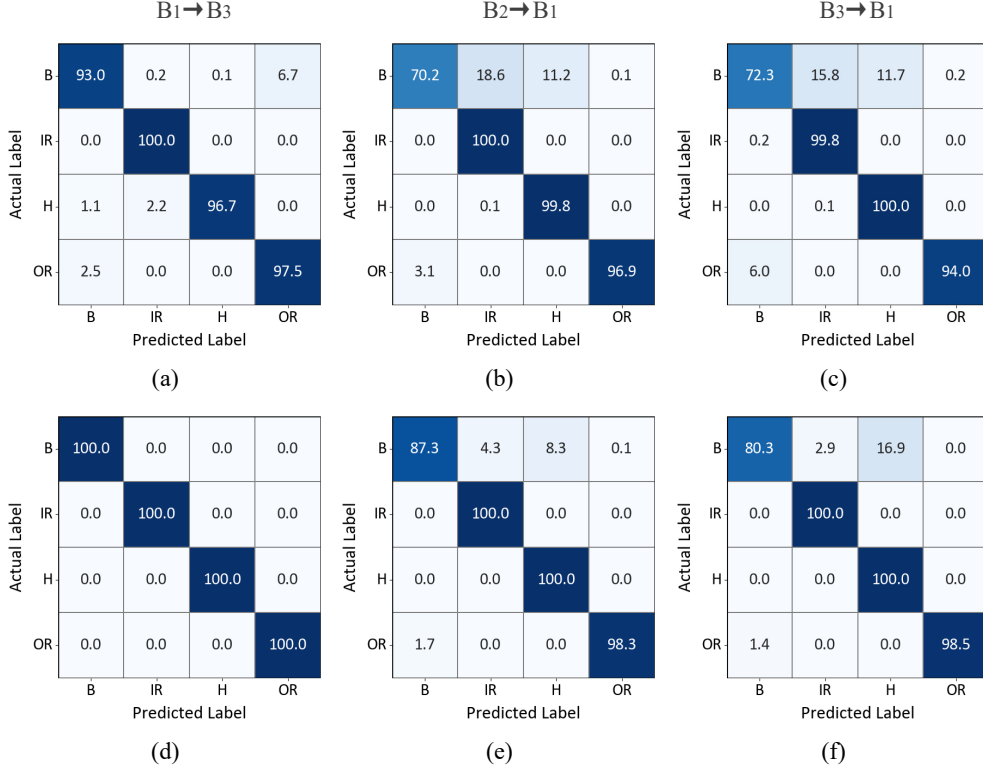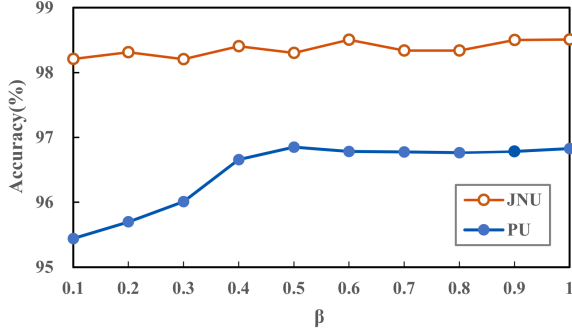
Figure 8: Confusion matrix comparison of SF-CA and SDALR on JNU datasets to evaluate classification performance across different tasks. Subplot (a)(b)(c) represent the confusion matrices of the SF-CA method, while subplot (d)(e)(f) correspond to the confusion matrices of the SDALR method

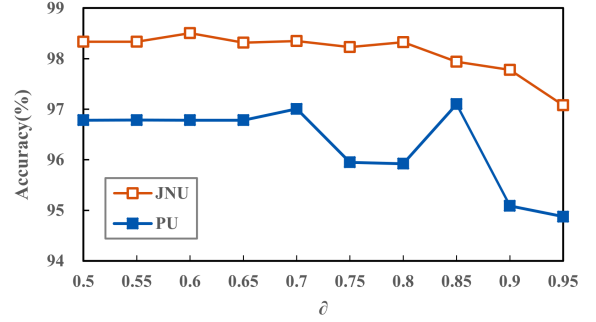Figure 9: Bearing fault diagnosis accuracy curves for hyper-parameter β.

Figure 10: Bearing fault diagnosis accuracy curves for hyper-parameter ∂.

(L_{uem}). To evaluate the effectiveness of each module, we conducted an ablation study. In the initial experiment, cohesion and repulsion loss (L_{car}), pseudo-label voting (voting), and entropy maximization loss (L_{uem}) were removed, leaving only label-smoothing cross-Entropy loss (L_{lsc}) and information maximization loss (L_{im}) as the baseline method. This configuration is analogous to the SHOT method. Subsequently, the modules were added incrementally to assess their contributions to improving model performance.

The detailed results of the ablation study on two datasets are presented in Table 6 and Table 7. Comparative analysis indicates that the model's diagnostic performance improves with the inclusion of each additional module. These findings highlight the positive contributions of each component to the overall perfor-

mance, validating the proposed approach and supporting the rationality of its modular design.
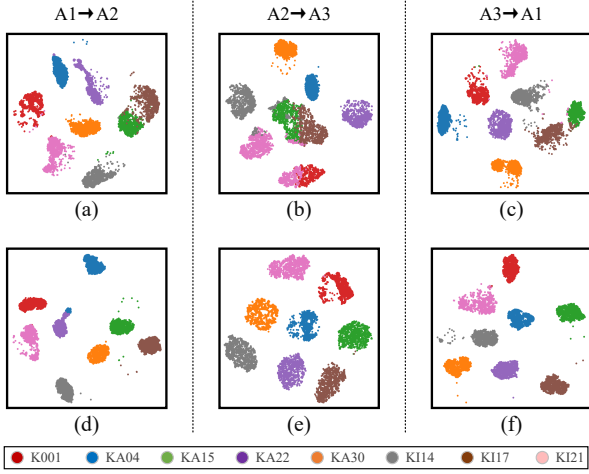
4.5.4. Visualization

Figure 11: Qualitative visualization using t-SNE to illustrate the distribution patterns across PU datasets from different domains. Subplot (a)(b)(c) represent the visualization results of SF-CA, while subplot (d)(e)(f) represent the visualization results of SDALR.
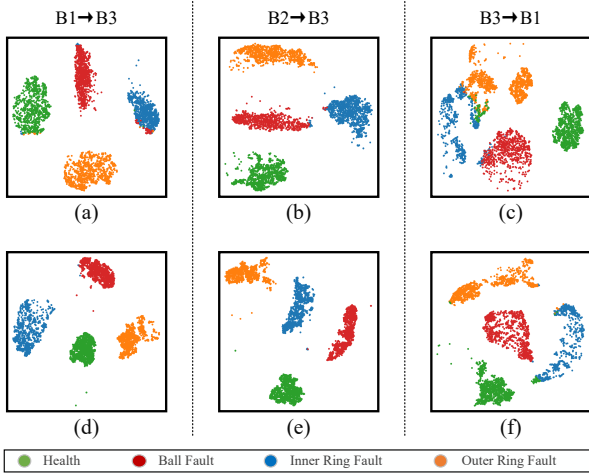

Figure 12: Qualitative visualization using t-SNE to illustrate the distribution patterns across PU datasets from different domains. Subplot (a)(b)(c) represent the visualization results of SF-CA, while subplot (d)(e)(f) represent the visualization results of SDALR.

To gain deeper qualitative insights, feature representations were visualized using t-SNE, focusing on the performance of SDALR and the state-of-the-art model SF-CA on two datasets. Tasks $A_1{\rightarrow}A_2$, $A_2{\rightarrow}A_3$, $A_3{\rightarrow}A_1$, $B_1{\rightarrow}B_3$, $B_2{\rightarrow}B_3$, $B_3{\rightarrow}B_1$ were selected for

evaluation. Figures 11 and 12 display the feature representations extracted from the final layer of the feature encoder, where different colors correspond to different categories. For the PU dataset, the visualizations cover eight bearing states, while for the JNU dataset, four bearing states are depicted. Unlike traditional unsupervised domain adaptation methods that align features between source and target domains, this study focuses solely on target-domain features due to the source-free adaptation setup. The results show that SDALR learns distinct and well-separated feature representations for each category, enabling precise fault diagnostics. In contrast, SF-CA exhibits less clear class separation. These findings confirm that SDALR achieves superior feature learning, further validating its effectiveness over SF-CA.

5. Conclusion

This paper proposes an innovative SFDA method to address three core challenges in source-free cross-domain bearing fault diagnosis: ensuring discriminability, and diversity in the feature space, improving pseudo-label quality and reducing negative transfer from unreliable target samples. The approach integrates pseudo-label-guided clustering for feature structuring, a data-augmentation-based voting strategy for reliable pseudo-labels, and entropy maximization to minimize the impact of unreliable samples. Experimental results show that the method outperforms state-of-the-art methods in source-free cross-domain fault diagnosis.

While effective, the method's success heavily depends on the quality of the source model. Future work should enhance source model generalization, leverage reliable information to improve adaptability, and extend this approach to dynamic adaptation scenarios and complex industrial applications for broader relevance.

Declaration of competing interest

The authors declare that they have no known competing financial interests or personal relationships that could have appeared to influence the work reported in this paper.

Table 6: Results(%) of Ablation Studies in PU

Methods	$A_1 \rightarrow A_2$	$A_1 \rightarrow A_3$	$A_2 \rightarrow A_1$	$A_2 \rightarrow A_3$	$A_3 \rightarrow A_1$	$A_3 \rightarrow A_2$	Average
$L_{lsc} + L_{im}$	86.41	94.58	82.58	85.12	92.95	87.88	88.25
$L_{lsc} + L_{im} + L_{car}$	87.05	99.99	87.38	99.63	99.97	97.51	95.26
$L_{lsc} + L_{im} + L_{car}$ + Voting	87.62	99.98	87.88	99.89	99.97	97.68	95.50
$L_{lsc} + L_{im} + L_{car}$ + Voting + L_{uem}	87.03	99.95	96.19	99.73	99.96	97.84	96.78

Table 7: Results(%) of Ablation Studies in JNU

Methods	$B_1 \rightarrow B_2$	$B_1 \rightarrow B_3$	$B_2 \rightarrow B_1$	$B_2 \rightarrow B_3$	$B_3 \rightarrow B_1$	$B_3 \rightarrow B_2$	Average
$L_{lsc} + L_{im}$	94.31	88.35	90.27	84.37	92.05	97.29	91.11
$L_{lsc} + L_{im} + L_{car}$	99.98	100.00	96.04	99.99	93.66	99.94	98.27
$L_{lsc} + L_{im} + L_{car}$ + Voting	99.96	100.00	96.34	99.99	94.49	99.95	98.46
$L_{lsc} + L_{im} + L_{car}$ + Voting + L_{uem}	99.98	100.00	96.41	100.00	94.71	99.92	98.50

References

[1] J. Singh, M. Azamfar, F. Li, J. Lee, A systematic review of machine learning algorithms for prognostics and health management of rolling element bearings: fundamentals, concepts and applications, Measurement Science and Technology 32 (1) (2020) 012001.

[2] Z. Ye, J. Yu, Multi-level features fusion network-based feature learning for machinery fault diagnosis, Applied Soft Computing 122 (2022) 108900.

[3] Y. Wu, C. Li, S. Yang, Y. Bai, Multiscale reduction clustering of vibration signals for unsupervised diagnosis of machine faults, Applied Soft Computing 142 (2023) 110358.

[4] H. Cao, L. Niu, S. Xi, X. Chen, Mechanical model development of rolling bearing-rotor systems: A review, Mechanical Systems and Signal Processing 102 (2018) 37–58.

[5] Z. Li, H. Zhang, X.-Y. Jing, J. Xie, M. Guo, J. Ren, Dssdpp: data selection and sampling based domain programming predictor for cross-project defect prediction, IEEE Transactions on Software Engineering 49 (4) (2022) 1941–1963.

[6] L. Shu, Y. Chen, Z. Sun, F. Tong, M. Mukherjee, Detecting the dangerous area of toxic gases with wireless sensor networks, IEEE Transactions on Emerging Topics in Computing 8 (1) (2017) 137–147.

[7] D.-T. Hoang, H.-J. Kang, A survey on deep learning based bearing fault diagnosis, Neurocomputing 335 (2019) 327–335.

[8] H. Chen, X.-Y. Jing, Y. Zhou, B. Li, B. Xu, Aligned metric representation based balanced multiset ensemble learning for heterogeneous defect prediction, Information and Software Technology 147 (2022) 106892.

[9] F. Zhuang, Z. Qi, K. Duan, D. Xi, Y. Zhu, H. Zhu, H. Xiong, Q. He, A comprehensive survey on transfer learning, Proceedings of the IEEE 109 (1) (2020) 43–76.

[10] H. Yan, Y. Ding, P. Li, Q. Wang, Y. Xu, W. Zuo, Mind the class weight bias: Weighted maximum mean discrepancy for unsupervised domain adaptation, in: Proceedings of the IEEE conference on computer vision and pattern recognition, 2017, pp. 2272–2281.

[11] A. T. Nguyen, T. Tran, Y. Gal, P. H. Torr, A. G. Baydin, Kl guided domain adaptation, arXiv preprint arXiv:2106.07780 (2021).

[12] J. Shen, Y. Qu, W. Zhang, Y. Yu, Wasserstein distance guided representation learning for domain adaptation, in: Proceedings of the AAAI conference on artificial intelligence, Vol. 32, 2018.

[13] B. Benjdira, Y. Bazi, A. Koubaa, K. Ouni, Unsupervised domain adaptation using generative adversarial networks for semantic segmentation of aerial images, Remote Sensing 11 (11) (2019) 1369.

[14] A. Farahani, S. Voghoei, K. Rasheed, H. R. Arabnia, A brief review of domain adaptation, Advances in data science and information engineering: proceedings from ICDATA 2020 and IKE 2020 (2021) 877–894.

[15] S. Tang, S. Yuan, Y. Zhu, Deep learning-based intelligent fault diagnosis methods toward rotating machinery, Ieee Access 8 (2019) 9335–9346.

[16] Y. Kim, D. Cho, K. Han, P. Panda, S. Hong, Domain adaptation without source data, IEEE Transactions on Artificial Intelligence 2 (6) (2021) 508–518.

[17] Z. Zhang, W. Chen, H. Cheng, Z. Li, S. Li, L. Lin, G. Li, Divide and contrast: Source-free domain adaptation via adaptive contrastive learning, Advances in Neural Information Processing Systems 35 (2022) 5137–5149.

[18] S. Yang, Y. Wang, J. Van De Weijer, L. Herranz, S. Jui, Generalized source-free domain adaptation, in: Proceedings of the IEEE/CVF international conference on computer vision, 2021, pp. 8978–8987.

[19] Y. Fang, P.-T. Yap, W. Lin, H. Zhu, M. Liu, Source-free unsupervised domain adaptation: A survey, Neural Networks (2024) 106230.

[20] J. Liang, D. Hu, J. Feng, Do we really need to access the source data? source hypothesis transfer for unsupervised domain adaptation, in: International conference on machine learning, PMLR,

2020, pp. 6028–6039.

[21] M. P. Kumar, Z.-X. Tu, H.-C. Chen, K.-C. J. Chen, Mitigating negative transfer learning in source free-unsupervised domain adaptation for rotating machinery fault diagnosis, IEEE Transactions on Instrumentation and Measurement (2024).

[22] W. Jianyu, H. Zhang, M. Qiang, Source free unsupervised domain adaptation for electro-mechanical actuator fault diagnosis, Chinese Journal of Aeronautics 36 (4) (2023) 252–267.

[23] M. Zhu, X. Zeng, J. Liu, C. Yang, K. Zhou, Source-free cluster adaptation for privacy-preserving machinery fault diagnosis, IEEE Transactions on Instrumentation and Measurement (2023).

[24] Q. Li, B. Tang, L. Deng, P. Zhu, Source-free domain adaptation framework for fault diagnosis of rotation machinery under data privacy, Reliability Engineering & System Safety 238 (2023) 109468.

[25] Z. Cai, T. Zhang, F. Ma, X.-Y. Jing, Dual contrastive universal adaptation network for multi-source visual recognition, Knowledge-Based Systems 254 (2022) 109632.

[26] S. J. Pan, I. W. Tsang, J. T. Kwok, Q. Yang, Domain adaptation via transfer component analysis, IEEE transactions on neural networks 22 (2) (2010) 199–210.

[27] B. Sun, K. Saenko, Deep coral: Correlation alignment for deep domain adaptation, in: Computer Vision–ECCV 2016 Workshops: Amsterdam, The Netherlands, October 8-10 and 15-16, 2016, Proceedings, Part III 14, Springer, 2016, pp. 443–450.

[28] W. Qian, S. Li, X. Jiang, Deep transfer network for rotating machine fault analysis, Pattern recognition 96 (2019) 106993.

[29] F. Ferracuti, A. Freddi, A. Monteriù, L. Romeo, Fault diagnosis of rotating machinery based on wasserstein distance and feature selection, IEEE Transactions on Automation Science and Engineering 19 (3) (2021) 1997–2007.

[30] J. Chen, J. Wang, J. Zhu, T. H. Lee, C. W. de Silva, Unsupervised cross-domain fault diagnosis using feature representation alignment networks for rotating machinery, IEEE/ASME Transactions on Mechatronics 26 (5) (2020) 2770–2781.

[31] X. Li, Y. Hu, J. Zheng, M. Li, W. Ma, Central moment discrepancy based domain adaptation for intelligent bearing fault diagnosis, Neurocomputing 429 (2021) 12–24.

[32] E. Tzeng, J. Hoffman, K. Saenko, T. Darrell, Adversarial discriminative domain adaptation, in: Proceedings of the IEEE Conference on Computer Vision and Pattern Recognition (CVPR), 2017.

[33] Y. Wang, X. Sun, J. Li, Y. Yang, Intelligent fault diagnosis with deep adversarial domain adaptation, IEEE Transactions on Instrumentation and Measurement 70 (2020) 1–9.

[34] J. Kuang, G. Xu, T. Tao, S. Zhang, Self-supervised bi-classifier adversarial transfer network for cross-domain fault diagnosis of rotating machinery, ISA transactions 130 (2022) 433–448.

[35] B. Zhao, X. Zhang, Z. Zhan, Q. Wu, Deep multi-scale adversarial network with attention: A novel domain adaptation method for intelligent fault diagnosis, Journal of Manufacturing Systems 59 (2021) 565–576.

[36] J. Jiao, J. Lin, M. Zhao, K. Liang, C. Ding, Cycle-consistent adversarial adaptation network and its application to machine fault diagnosis, Neural Networks 145 (2022) 331–341.

[37] W. Mao, Y. Liu, L. Ding, A. Safian, X. Liang, A new structured domain adversarial neural network for transfer fault diagnosis of rolling bearings under different working conditions, IEEE Transactions on Instrumentation and Measurement 70 (2020) 1–13.

[38] Y. Zhou, Y. Dong, H. Zhou, G. Tang, Deep dynamic adaptive transfer network for rolling bearing fault diagnosis with considering cross-machine instance, IEEE Transactions on Instrumentation and Measurement 70 (2021) 1–11.

[39] C. J. Hoofnagle, B. Van Der Sloot, F. Z. Borgesius, The european union general data protection regulation: what it is and what it means, Information & Communications Technology Law 28 (1) (2019) 65–98.

[40] J. Chen, J. Sun, Understanding the chinese data security law, International Cybersecurity Law Review 2 (2) (2021) 209–221.

[41] J. Jiao, H. Li, T. Zhang, J. Lin, Source-free adaptation diagnosis for rotating machinery, IEEE Transactions on Industrial Informatics 19 (9) (2022) 9586–9595.

[42] M. Zhu, X. Zeng, J. Liu, K. Zhou, Source-free unsupervised domain adaptation for privacy-preserving intelligent fault diagnosis, in: 2022 International Conference on Sensing, Measurement & Data Analytics in the era of Artificial Intelligence (ICSMD), IEEE, 2022, pp. 1–6.

[43] K. Yue, W. Li, J. Li, Z. Chen, R. Huang, Source-free partial domain adaptation in rotating machinery fault diagnosis using deep hypothesis domain adaptation network, in: 2022 International Conference on Sensing, Measurement & Data Analytics in the era of Artificial Intelligence (ICSMD), IEEE, 2022, pp. 1–6.

[44] Y. Zhang, Z. Ren, K. Feng, K. Yu, M. Beer, Z. Liu, Universal source-free domain adaptation method for cross-domain fault diagnosis of machines, Mechanical Systems and Signal Processing 191 (2023) 110159.

[45] J. Li, K. Yue, R. Huang, Z. Chen, K. Gryllias, W. Li, Unsupervised continual source-free network for fault diagnosis of machines under multiple diagnostic domains, IEEE Sensors Journal 23 (8) (2023) 8292–8303.

[46] J. Zhang, Z. Jiang, L. Zhang, Source-free domain adaptation for rotating machinery cross-domain fault diagnosis with neighborhood reciprocity clustering, in: 2022 China Automation Congress (CAC), IEEE, 2022, pp. 5333–5340.

[47] C. Lessmeier, J. K. Kimotho, D. Zimmer, W. Sextro, Condition monitoring of bearing damage in electromechanical drive systems by using motor current signals of electric motors: A benchmark data set for data-driven classification, in: PHM Society European Conference, Vol. 3, 2016.

[48] K. Li, X. Ping, H. Wang, P. Chen, Y. Cao, Sequential fuzzy diagnosis method for motor roller bearing in variable operating conditions based on vibration analysis, Sensors 13 (6) (2013) 8013–8041.

[49] M. Long, H. Zhu, J. Wang, M. I. Jordan, Deep transfer learning with joint adaptation networks, in: International conference on machine learning, PMLR, 2017, pp. 2208–2217.

[50] Y. Ganin, E. Ustinova, H. Ajakan, P. Germain, H. Larochelle, F. Laviolette, M. March, V. Lempitsky, Domain-adversarial training of neural networks, Journal of machine learning research 17 (59) (2016) 1–35.

15